

Single crystal growth and study of the ferromagnetic superconductor $\text{RbEuFe}_4\text{As}_4$

Jin-Ke Bao¹, Kristin Willa¹, Matthew P. Smylie¹, Haijie Chen^{1, 2}, Ulrich Welp¹, Duck Young Chung¹, and Mercuri G. Kanatzidis^{1, 2, *}

¹*Materials Science Division, Argonne National Laboratory, Argonne, Illinois 60439, United States,* ²*Department of Chemistry, Northwestern University, Evanston, Illinois 60208, United States.*

SYNOPSIS:

High quality single crystals of ferromagnetic superconductor $\text{RbEuFe}_4\text{As}_4$ were successfully grown using RbAs flux giving samples with a sharp superconducting transition at ~ 36.8 K. Our study points out a robust method to grow and explore other compounds using the same flux.

ABSTRACT:

$\text{RbEuFe}_4\text{As}_4$ exhibits both superconducting order in the FeAs layers and ferromagnetic order in the Eu layers providing a good platform to study the interaction and microscopic coexistence of these two traditionally incompatible orders. Synthesizing high quality $\text{RbEuFe}_4\text{As}_4$ single crystals is essential to investigate these phenomena at a deeper level. Here we report the successful growth of $\text{RbEuFe}_4\text{As}_4$ single crystals with millimeter-size dimensions using RbAs flux. The high quality crystals were characterized via resistivity, magnetization and heat capacity measurements. Single crystal x-ray diffraction data refinements reveal almost regular FeAs₄ tetrahedra ($\text{As1-Fe-As1} = 108.60(7)^\circ$, $\text{As2-Fe-As2} = 109.01(8)^\circ$ and $\text{As1-Fe-As2} = 109.81(2)^\circ$) in $\text{RbEuFe}_4\text{As}_4$, providing structural support for the highest superconducting transition temperature ($T_c = 36.8$ K) among all known $A\text{AeFe}_4\text{As}_4$ ($A = \text{K, Rb, Cs}$; $\text{Ae} = \text{Ca, Sr, Eu}$) compounds. Our flux method using RbAs can also be employed to grow other desired transition metal compounds targeting the same crystal structure.

INTRODUCTION

Since the discovery of iron-based superconductivity in 2008,¹ the unusually high transition temperature and unconventional nature of superconductivity has generated great interest among researchers in this field². To reveal its intrinsic properties in depth and further resolve the mechanism of superconductivity, synthesizing high quality single crystals of the materials is crucial. Large and high quality single crystals of 122 compounds $AeFe_2As_2$ ($Ae = Ba, Sr, Ca, Eu$) can be easily grown by binary fluxes³ while it is not easy to grow single crystals with large dimensions of $LnFeAsO$ ($Ln = La, Ce, Pr, etc$)⁴. As such, more detailed investigations of the $LnFeAsO$ family are still limited despite the much higher superconducting transition temperatures therein as compared to the $AeFe_2As_2$ family.⁵

Recently, the $AAeFe_4As_4$ ($A = K, Rb, Cs$) family, a new type of iron-based superconductor, so-called the 1144 phase, was reported by Iyo *et al.* with an ordered stacking of A^+ and Ae^{2+} cations between FeAs layers along the c axis, see Figure 1(a).⁶ They adopt the simple tetragonal $P4/mmm$ space group, different from the body-centered tetragonal $I4/mmm$ found in the hole doped 122 superconductor $Ba_{1-x}K_xFe_2As_2$. The radius difference between A^+ and Ae^{2+} cations and the lattice match of the ternary compounds AFe_2As_2 and $AeFe_2As_2$ are important to stabilize this structure.⁶ In the new structure, the FeAs₄ tetrahedron is only slightly distorted with two crystallographic sites As1 and As2 providing two angles: As1-Fe-As1 (α_1) and As2-Fe-As2 (α_2), see Figure 1(a) and (b), in contrast to the single As site and As-Fe-As angle in the common 122 superconductors.

It is important to grow large enough single crystal samples to further study their physical properties of $AAeFe_4As_4$ especially in view of the thermal stability of the two ternary compounds AFe_2As_2 and $AeFe_2As_2$, which compete in the reaction chemistry and make it difficult to allow the quaternary $AAeFe_4As_4$ single crystals to form.⁶ Recently, single crystals of $CaKFe_4As_4$ were successfully grown with no impurity ternary phases by Meier *et al*⁷ using FeAs flux, which enabled detailed investigations on the superconducting properties of this compound.⁸⁻¹⁶

Among the new 1144 type compounds, $AEuFe_4As_4$ is unique because of the extra magnetic sublattice from a plane of Eu^{2+} ions.¹⁷⁻¹⁹ Ferromagnetism and superconductivity appear in Eu sublattices and FeAs layers of $AEuFe_4As_4$, respectively.^{17, 19} Those two orders are generally mutually antagonistic²⁰, which makes $AEuFe_4As_4$ an interesting system to study the coexistence and mutual interaction of these orders in a single structure. Up until now, no single crystals of

$A\text{EuFe}_4\text{As}_4$ have been successfully grown. In this study, we have successfully grown high quality $\text{RbEuFe}_4\text{As}_4$ single crystals using RbAs flux. The quality of the crystals was assessed by resistivity, magnetization and specific heat measurements. We observe that a very thin film RbFe_2As_2 forms on the (001) surface of $\text{RbEuFe}_4\text{As}_4$, but can be cleaved off and has almost no influence on the physical properties measured for this compound.

EXPERIMENTAL SECTION

Synthesis

As starting reagents for reactions, Rb metal sealed under argon (99%, Johnson Matthey), Eu chunks (99.9%, Alfa Aesar), Fe powder (99.998%, Alfa Aesar) and As powder (99.9999%, Alfa Aesar) were used. All reactions were carried out in an evacuated fused silica tube sealed under a vacuum below 10^{-3} mbar. RbAs was synthesized by a direct reaction of Rb (0.8427 g, 9.9 mmol) and As (0.7035 g, 9.4 mmol) powder in an alumina crucible (ID = 8 mm) with a nominal composition $\text{Rb}_{1.05}\text{As}$. A small excess of Rb was used to compensate for evaporation loss during the process. The mixture was heated in a vacuum sealed silica tube (15 mm OD, 13 mm ID) to 443 K over 24 hours and held there for 12 hours. EuAs was synthesized separately by loading small Eu pieces (1.2 g, 7.9 mmol) and As powder (0.5633 g, 7.5 mmol) with a nominal composition $\text{Eu}_{1.05}\text{As}$ into a silica tube, which was evacuated and slowly heated to 973 K and held there for 24 hours. Fe_2As was synthesized by a homogenized mixture of Fe powder (1.5 g, 26 mmol) and As powder (1.007 g, 13 mmol) in a silica tube, which was heated at 1023 K for 24 hours. EuFe_2As_2 was synthesized by mixing EuAs and Fe_2As in a 1:1 ratio (total mass ~ 0.54 g) in an evacuated silica tube and heating the mixture up at 1073 K for 24 hours.

A mixture of RbAs , Fe_2As and EuAs in a ratio of 15:1:1 with a total amount ~ 2 g were homogenized in an agate mortar and then loaded into an alumina crucible. The alumina crucible containing the mixture was then sealed in a Nb tube under argon atmosphere by arc welding. Finally, the Nb tube was sealed in a larger silica tube (18 mm OD, 16 mm ID), see the diagram of the tube assembly in Figure 2(a). The tube was heated to 1193 K over 20 hours, held for 12 hours and then cooled to 823 K at a rate of 2 K/h, after which the furnace was shut down. RbAs flux in the final product was washed out by reagent alcohol in a fume hood under a N_2 flow. A toxic gas, AsH_3 , was released in this process, which requires special caution, requiring the fume hood. The crystals soaked in the reagent alcohol were washed in an ultrasonic bath to remove the impurity

particles on the crystal surface. Shiny square crystals with a millimeter-size dimension were harvested, see Figure 2(b). The crystals grown under the ratio $\text{RbAs} : \text{EuFe}_2\text{As}_2 = 5:1$ were much smaller than those from the ratio mentioned above, see Figure S1 in *Supporting Information*. The crystal samples used for characterization of the compound $\text{RbEuFe}_4\text{As}_4$ in this article are from the ratio $\text{RbAs} : \text{Fe}_2\text{As} : \text{EuAs} = 15:1:1$.

Single and powder x-ray diffraction

A crystal of $\text{RbEuFe}_4\text{As}_4$ with dimensions of $\sim 0.210 \times 0.163 \times 0.090 \text{ mm}^3$ was selected for single x-ray diffraction study using a STOE IPDS 2T diffractometer at room temperature. Data collection, reduction, integration, and absorption correction were performed using the X-area software package.²¹ The structure was solved and refined based on the full matrix least-squares algorithm of F^2 by using the SHLEXTL program package.²² The overall refinement results of $\text{RbEuFe}_4\text{As}_4$ are shown in Table 1. $\text{RbEuFe}_4\text{As}_4$ crystallizes in a tetragonal structure with a space group $P4/mmm$. The $(hk4)$ reciprocal lattice plane reflection data exhibit tetragonal symmetry and no systematic absences, consistent with the $P4/mmm$ space group, see Figure 2(c). Table 2 shows the atomic coordinates and their isotropic thermal displacement parameters. Detailed anisotropic displacements as well as bond length and angles are shown in Tables S2 and S3 in the *Supporting Information*. The refined lattice parameters and atomic coordinates shown in Table 1 and 2 are in good agreement with previous reports on polycrystalline material.^{17, 18} Powder x-ray diffraction of the crystals was conducted using a PANalytical diffractometer X'pert with a Cu K_α radiation.

Scanning electron microscopy and energy dispersive x-ray spectroscopy

Surface imaging and the elemental analysis of $\text{RbEuFe}_4\text{As}_4$ crystals were performed using a Hitachi S-4700-II scanning electron microscope (SEM) equipped with an energy dispersive x-ray spectroscopy (EDS) detector. The samples were mounted on an aluminum sample stub with carbon tape. The acceleration voltage and beam current for the measurements were 20 keV and 10 μA , respectively. EDS analysis on multiple crystals cleaved with a fresh surface gave an average composition, $\text{Rb}_{1.07(3)}\text{Eu}_{0.91(5)}\text{Fe}_4\text{As}_{3.90(3)}$, consistent with the stoichiometric composition $\text{RbEuFe}_4\text{As}_4$.

Transport property measurements

Temperature dependence of resistivity and Hall effect measurements were performed on a commercial physical property measurement system (Dynacool, Quantum Design). Gold wires

were attached to the as-grown crystal by silver paste (Dupont 4929N). The magnetic fields were applied perpendicular to *ab* plane. Due to the unavoidable tiny misalignment of the Hall contacts, a magnetoresistance component was removed from the Hall resistivity by scanning magnetic fields from -9 to 9 T and further making a subtraction between positive and negative fields.

Magnetic susceptibility measurements

Temperature dependence of magnetic susceptibility was measured on a commercial magnetic property measurement system (MPMS3, Quantum Design). One as-grown crystal $\text{RbEuFe}_4\text{As}_4$ ($\sim 0.4 \times 0.4 \times 0.08 \text{ mm}^3$) was mounted on a silica sample holder with a minimal amount of GE varnish. Magnetic fields were applied along the *ab* plane. Demagnetization factors were considered in evaluating the superconducting volume fraction of the sample $\text{RbEuFe}_4\text{As}_4$.²³ The crystal was too light to measure the mass accurately. Instead, its volume was measured to calculate its molar magnetic susceptibility and superconducting volume fraction.

AC specific heat measurements

Specific heat measurements were carried out by a membrane-based (silicon nitride) ac nanocalorimeter.^{24, 25} Flat square shaped crystals (approximately $80 \times 80 \times 20 \text{ }\mu\text{m}^3$) were mounted onto the membrane with Apiezon grease and subsequently cooled down in vacuum. Measurements were performed with a Synkex MCL1-540 multi-channel lock-in system. Operating frequencies were around 1Hz.

RESULTS AND DISCUSSION

Crystal growth

RbAs is an effective flux to grow arsenide compounds²⁶ because it has relatively low melting temperature (848 K) and high reactivity. However, the high reactivity of RbAs also causes a side reaction with the silica tube used as a container. We examined the thermal stability of $\text{RbEuFe}_4\text{As}_4$ in the silica tube by annealing at 1173 K and observed that a polycrystalline powder sample of $\text{RbEuFe}_4\text{As}_4$ in a silica tube decomposes into EuFe_2As_2 and FeAs , see Figure S2. Therefore, the use of Nb or other metal tubes was necessary to prevent unintentional loss of RbAs flux that can change the original stoichiometry, as shown in Figure 2(a). For the crystal growth of $\text{RbEuFe}_4\text{As}_4$, we initially attempted the ratio $\text{RbAs}:\text{EuFe}_2\text{As}_2 = 5:1$ which produced very small $\text{RbEuFe}_4\text{As}_4$ crystals ($\sim 0.2 \times 0.2 \times 0.05 \text{ mm}^3$), see Figure S1. This product also contained a small amount ($\sim 4\%$

in mass) of EuFe_2As_2 impurities detected by sensitive ac nanocalorimeter measurements (see Figure S3) indicating that the precursor compound EuFe_2As_2 was not fully dissolved in the RbAs flux in that ratio. According to the binary Eu-As phase diagram²⁷, the binary phases EuAs_x have high melting points, implying that the solubility of elemental Eu in RbAs may not be high. Thus, we increased the RbAs flux ratio to 15:1 and used binary precursors instead of the ternary precursor EuFe_2As_2 , by which large crystals with a millimeter-size dimension were successfully harvested, see Figure 2(b).

Crystal structure and morphology

The structure of the $\text{RbEuFe}_4\text{As}_4$ crystals was solved and refined accurately as shown in Table 1. The unit cell consists of stacked FeAs layers which are sandwiched by Eu and Rb layers alternating along the c axis, see Figure 1(a). Each FeAs layer consists of edge sharing FeAs_4 tetrahedra. Each Rb atom is coordinated with eight As1 atoms in a rectangular prism and each Eu atom is bonded with eight As2 atoms in a similar coordination geometry. The As1-Fe-As1 angle (α_1 , $108.60(7)^\circ$) in the FeAs_4 tetrahedron is not strictly equal to but is very close to As2-Fe-As2 (α_2 , $109.01(8)^\circ$) and As1-Fe-As2 (β , $109.81(2)^\circ$) to form a nearly regular tetrahedron in $\text{RbEuFe}_4\text{As}_4$, see Table S2. We verified these angles in the refined structures of three other crystals, see Table S3. A useful empirical rule in evaluating T_c in iron arsenide-based superconductors is that a high regularity of the FeAs_4 tetrahedra in FeAs layers always give rise to high T_c .²⁸ Our single crystal refinements on $\text{RbEuFe}_4\text{As}_4$ crystals reveal almost regular FeAs_4 tetrahedra ($\alpha_1 \approx \alpha_2 \approx \beta$) in the FeAs layers, which supports the observation that $\text{RbEuFe}_4\text{As}_4$ has the highest superconducting transition temperature ($T_c = 36.8$ K) among the known 1144 superconductors.

The morphology of $\text{RbEuFe}_4\text{As}_4$ crystals is square or rectangular plates, Figure 2(b). A typical as-grown single crystal plate in a powder x-ray diffractometer shows two series of Bragg peaks, Figure 3(a). One set of peaks indexed as $(0\ 0\ l)$ basal reflections matches well the phase $\text{RbEuFe}_4\text{As}_4$. The other set of peaks indexed with $(0\ 0\ 2l)$ give a larger c axis ($c \sim 14.38$ Å), which is consistent with the c axis of I -centered RbFe_2As_2 .²⁹ This indicates that a very thin film of RbFe_2As_2 has grown epitaxially on the (001) surface of $\text{RbEuFe}_4\text{As}_4$ sharing the same c axis orientation and having latticed matched ab planes ($a \sim 3.87$ Å) of RbFe_2As_2 and ($a \sim 3.88$ Å) of $\text{RbEuFe}_4\text{As}_4$. As a result, the RbFe_2As_2 phase tends to grow as a deposited film on the (001) surface of $\text{RbEuFe}_4\text{As}_4$ crystals that seems to happen at the end of the growth process. SEM image of

pristine crystals clearly shows the roughness and tiny holes on the surface caused by the thin layer of RbFe_2As_2 , see Figure S4. Due to the quasi-two-dimensional bonding characteristics in $\text{RbEuFe}_4\text{As}_4$, the thin RbFe_2As_2 film can be easily removed by cleaving the crystal along the c axis using a carbon tape, see Figure 3(b).

The possible crystal growth process of $\text{RbEuFe}_4\text{As}_4$ in a ratio of $\text{RbAs}:\text{EuAs}:\text{Fe}_2\text{As} = 15:1:1$ is summarized as a schematic diagram, see Figure 4. During the cooling process from the highest temperature (1193 K), $\text{RbEuFe}_4\text{As}_4$ single crystals first crystallize out of the solution below a certain temperature T_1 and then below another temperature T_2 RbFe_2As_2 phase crystallizes out of solution. Because of the good lattice match between $\text{RbEuFe}_4\text{As}_4$ and RbFe_2As_2 , the grown crystals $\text{RbEuFe}_4\text{As}_4$ act as the seed crystals for RbFe_2As_2 to grow epitaxially below T_2 . The as-grown crystals are of high quality as judged by the physical property measurements. The very thin film of RbFe_2As_2 deposited on the top surface of $\text{RbEuFe}_4\text{As}_4$ crystals has almost no influence on the superconducting properties measurements, as will be shown below. Clean pristine $\text{RbEuFe}_4\text{As}_4$ crystals without a thin RbFe_2As_2 film may be achieved by further modifying the cooling temperature window or the initial composition.

Superconducting properties

The quality and superconducting properties of the as-grown $\text{RbEuFe}_4\text{As}_4$ crystals was examined by basic transport, magnetization and specific heat measurements. The electrical resistivity of $\text{RbEuFe}_4\text{As}_4$ in the ab plane has a convex curvature from around 100 to 300 K, see Figure 5(a), similar to previous reports on polycrystalline samples.^{17, 18} The convex curvature is common in hole-doped iron-based superconductors, which may be related to multiband effects with asymmetric scatterings^{30, 31}. The resistivity at 300 K and residual resistivity ratio ($RRR = R_{300\text{K}}/R_{40\text{K}}$) for the $\text{RbEuFe}_4\text{As}_4$ crystal are 0.35 m Ω cm and 13, respectively. No obvious anomaly in the resistivity at around 195 K from EuFe_2As_2 ^{32, 33} impurity was observed in the resistivity, proving that the crystals are free of EuFe_2As_2 . A very sharp superconducting transition occurred at $T_{\text{onset}} = 37.1$ K and a zero resistivity temperature $T_{\text{zero}} = 36.8$ K, see the lower inset of Figure 5(a). The superconducting transition temperature window is only 0.3 K. The onset transition temperature of superconductivity in $\text{RbEuFe}_4\text{As}_4$ is only suppressed to 34 K when the magnetic field is increased to 9 T, indicating a very high upper critical field, see Figure 5(b). No reemergent resistivity was observed down to 2 K. The transverse resistivity ρ_{xy} increases linearly with magnetic fields above

100 K, confirming that hole carrier dominates the Hall effect, see Figure 5(c). The slopes of the $\rho_{xy}(H)$ curves changes with temperatures and shows the hole carrier concentration $\sim 10^{21}$ to 10^{22} cm^{-3} assuming a single band scenario.

Magnetic susceptibility of the $\text{RbEuFe}_4\text{As}_4$ crystal along the ab plane in a zero-field-cooled process presents a very sharp superconducting diamagnetic signal with an onset temperature $T_c = 36.8$ K, see Figure 6(a), consistent with the zero resistivity temperature mentioned above. Compared with the superconducting transitions from magnetic susceptibilities in the polycrystalline samples reported,^{17, 18} the transition in the single crystal is much sharper. The magnetic shielding volume observed is almost $\sim 100\%$, proving the bulk nature of superconductivity of the $\text{RbEuFe}_4\text{As}_4$ crystal. The magnetic repulsion volume is very small, which may be due to the strong flux pinning effect during the cooling process in a magnetic field. There is no observable superconducting signal from any RbFe_2As_2 ($T_c \sim 3$ K)²⁹ contaminant thin film on the surface of the crystal, indicating that the volume fraction of RbFe_2As_2 thin film is very small if any at all.

In addition to a superconducting transition in $\text{RbEuFe}_4\text{As}_4$, there is also a magnetic transition at $T_{\text{mag}} \sim 15$ K, which comes from the ordering of Eu magnetic sublattice. This transition temperature is consistent with previous reports on polycrystalline sample with a ferromagnetic behavior in the ab plane.^{17, 18} No anomaly at ~ 19 K or 195 K in magnetic susceptibilities from the EuFe_2As_2 phase³² are observed. Magnetic susceptibility of $\text{RbEuFe}_4\text{As}_4$ above 100 K can be fitted by a modified Curie-Weiss law

$$\chi = \chi_0 + \frac{C}{T - \theta}$$

where χ_0 is the temperature independent part, C is the Curie constant which is determined by effective magnetic moments of atoms, θ is the Curie-Weiss temperature indicating the interaction between individual magnetic moments, see Figure 6(b). The fitting gives $\chi_0 = 0.0128(1)$ emu/mol, $\theta = 17(1)$ K and $\mu_{\text{eff}} = 9.00(1)$ μ_{B}/Eu . The positive value of θ indicates a ferromagnetic interaction between Eu magnetic moments, consistent with the previous report on polycrystalline samples.¹⁷ The μ_{eff} obtained is slightly larger than the ideal Eu^{2+} one ($\mu_{\text{eff}} = 7.94$ μ_{B}/Eu), which may be related to experimental error in crystal volume measurements used for calculating molar magnetic susceptibility.

In order to further confirm the bulk nature of superconductivity and phase purity in RbEuFe₄As₄, specific heat measurements with an ac nanocalorimeter were conducted on the crystals, see Figure 7. Two phase transitions were observed, a specific heat jump at ~ 37 K and a cusp at ~ 15 K, corresponding to a superconducting transition of FeAs layers and a magnetic transition of the Eu sublattice, respectively, see the inset of Figure 7. The superconducting specific heat jump is quite sharp, demonstrating the high quality of the crystal. The magnetic transition of the Eu sublattice in the specific heat data is broad, indicating that short range magnetic correlations exists above the transition temperature, similar to previous polycrystalline samples¹⁷. No obvious anomaly at ~ 3 K was observed, further demonstrating that the film RbFe₂As₂ layer observed on the RbEuFe₄As₄ single crystal surface has no influence in this measurement.

CONCLUSION

We successfully grew well formed RbEuFe₄As₄ single crystals using RbAs flux. A very sharp superconducting transition at 36.8 K was observed by magnetic, transport and specific heat measurements, indicating a very high quality of the single crystal. We also confirm a magnetic transition at ~ 15 K that is associated with the ordering of Eu²⁺ sublattice. Though a thin layer of RbFe₂As₂ was observed on the surface of RbEuFe₄As₄ single crystals, this impurity phase does not influence the physical property characterization of the RbEuFe₄As₄ crystals and can also be removed by cleaving the as-grown crystals. Our single crystal refinements show a coordination geometry of FeAs₄ unit with two As-Fe-As angles very close to a regular tetrahedron in the FeAs layers, resulting in the highest superconducting transition temperature of RbEuFe₄As₄ among the known *AAe*Fe₄As₄ superconductors. The successful growth of RbEuFe₄As₄ single crystals can open that path to other detailed investigations with higher accuracy and reliability on this unique ferromagnetic superconductor. The formation of the ordered *AAe*Fe₄As₄ phase requires the *ab* plane lattice match between *A*Fe₂As₂ and *Ae*Fe₂As₂ as well as the large ionic radius difference between *A*⁺ and *Ae*²⁺.⁶ This hypothesis can also be extended to other transition metal compounds to design new phases. For example, the lattice parameters of RbRh₂As₂ (*a* = 3.994 Å)³⁴ and EuRh₂As₂ (*a* = 4.067 Å)³⁵ are quite similar, suggesting it is highly possible to synthesize RbEuRh₄As₄. Thus, we expect our method using RbAs flux can also be employed to explore other transition metal compounds RbEu*Tm*₄As₄ (*Tm* = transition metals).

ASSOCIATED CONTENT SUPPORTING INFORMATION.

This material is available free of charge via the Internet at <http://pubs.acs.org>.

Figure S1: powder x-ray diffraction of one typical crystal from the growth condition RbAs: EuFe₂As₂ = 5:1 from another batch. Figure S2: powder x-ray diffraction of annealed polycrystalline samples. Figure S3: specific heat data of one typical crystal from another batch. Figure S4: SEM images of crystals. Table S1 and S2: crystallographic information from the crystal in the main article. Table S3: FeAs₄ tetrahedron results from four crystals.

AUTHOR INFORMATION

Corresponding Author

*E-mail: m-kanatzidis@northwestern.edu

ACKNOWLEDGMENT

Work at Argonne National Laboratory was supported by the U.S. Department of Energy, Office of Science, Materials Sciences and Engineering. For EDS/SEM analysis, use of the Center for Nanoscale Materials, an Office of Science user facility, was supported by the U.S. Department of Energy, Office of Science, Office of Basic Energy Sciences, under Contract No. DE-AC02-06CH11357. The authors thank Dr. A. Koshchev for initiating the project of crystal growth of this material. The authors thank Yi Liu and Prof. Guang-Han Cao for providing the polycrystalline samples.

REFERENCES

- (1) Kamihara, Y.; Watanabe, T.; Hirano, M.; Hosono, H., *J. Am. Chem. Soc.* **2008**, 130, 3296-3297.
- (2) Johnston, D. C., *Adv. Phys.* **2010**, 59, 803-1061.
- (3) Sefat, A. S.; Jin, R.; McGuire, M. A.; Sales, B. C.; Singh, D. J.; Mandrus, D., *Phys. Rev. Lett.* **2008**, 101, 117004.

- (4) Yan, J. Q.; Nandi, S.; Zarestky, J. L.; Tian, W.; Kreyssig, A.; Jensen, B.; Kracher, A.; Dennis, K. W.; McQueeney, R. J.; Goldman, A. I.; McCallum, R. W.; Lograsso, T. A., *Appl. Phys. Lett.* **2009**, *95*, 222504.
- (5) Paglione, J.; Greene, R. L., *Nat. Phys.* **2010**, *6*, 645.
- (6) Iyo, A.; Kawashima, K.; Kinjo, T.; Nishio, T.; Ishida, S.; Fujihisa, H.; Gotoh, Y.; Kihou, K.; Eisaki, H.; Yoshida, Y., *J. Am. Chem. Soc.* **2016**, *138*, 3410-3415.
- (7) Meier, W. R.; Kong, T.; Bud'ko, S. L.; Canfield, P. C., *Phys. Rev. Mater.* **2017**, *1*, 013401.
- (8) Meier, W. R.; Kong, T.; Kaluarachchi, U. S.; Taufour, V.; Jo, N. H.; Drachuck, G.; Böhmer, A. E.; Saunders, S. M.; Sapkota, A.; Kreyssig, A.; Tanatar, M. A.; Prozorov, R.; Goldman, A. I.; Balakirev, F. F.; Gurevich, A.; Bud'ko, S. L.; Canfield, P. C., *Phys. Rev. B* **2016**, *94*, 064501.
- (9) Mou, D.; Kong, T.; Meier, W. R.; Lochner, F.; Wang, L.-L.; Lin, Q.; Wu, Y.; Bud'ko, S. L.; Eremin, I.; Johnson, D. D.; Canfield, P. C.; Kaminski, A., *Phys. Rev. Lett.* **2016**, *117*, 277001.
- (10) Biswas, P. K.; Iyo, A.; Yoshida, Y.; Eisaki, H.; Kawashima, K.; Hillier, A. D., *Phys. Rev. B* **2017**, *95*, 140505.
- (11) Bud'ko, S. L.; Kong, T.; Meier, W. R.; Ma, X.; Canfield, P. C., *Philos. Mag.* **2017**, *97*, 2689-2703.
- (12) Cho, K.; Fente, A.; Teknowijoyo, S.; Tanatar, M. A.; Joshi, K. R.; Nusran, N. M.; Kong, T.; Meier, W. R.; Kaluarachchi, U.; Guillamón, I.; Suderow, H.; Bud'ko, S. L.; Canfield, P. C.; Prozorov, R., *Phys. Rev. B* **2017**, *95*, 100502.
- (13) Cui, J.; Ding, Q. P.; Meier, W. R.; Böhmer, A. E.; Kong, T.; Borisov, V.; Lee, Y.; Bud'ko, S. L.; Valentí, R.; Canfield, P. C.; Furukawa, Y., *Phys. Rev. B* **2017**, *96*, 104512.
- (14) Fente, A.; Meier, W. R.; Kong, T.; Kogan, V. G.; Bud'ko, S. L.; Canfield, P. C.; Guillamon, I.; Suderow, H., *ArXiv: 1608.00605*.
- (15) Kaluarachchi, U. S.; Taufour, V.; Sapkota, A.; Borisov, V.; Kong, T.; Meier, W. R.; Kothapalli, K.; Ueland, B. G.; Kreyssig, A.; Valentí, R.; McQueeney, R. J.; Goldman, A. I.; Bud'ko, S. L.; Canfield, P. C., *Phys. Rev. B* **2017**, *96*, 140501.
- (16) Yang, R.; Dai, Y.; Xu, B.; Zhang, W.; Qiu, Z.; Sui, Q.; Homes, C. C.; Qiu, X., *Phys. Rev. B* **2017**, *95*, 064506.
- (17) Liu, Y.; Liu, Y.-B.; Tang, Z.-T.; Jiang, H.; Wang, Z.-C.; Ablimit, A.; Jiao, W.-H.; Tao, Q.; Feng, C.-M.; Xu, Z.-A.; Cao, G.-H., *Phys. Rev. B* **2016**, *93*, 214503.
- (18) Kawashima, K.; Kinjo, T.; Nishio, T.; Ishida, S.; Fujihisa, H.; Gotoh, Y.; Kihou, K.; Eisaki, H.; Yoshida, Y.; Iyo, A., *J. Phys. Soc. Jpn.* **2016**, *85*, 064710.
- (19) Liu, Y.; Liu, Y.-B.; Chen, Q.; Tang, Z.-T.; Jiao, W.-H.; Tao, Q.; Xu, Z.-A.; Cao, G.-H., *Sci. Bull.* **2016**, *61*, 1213-1220.
- (20) Bulaevskii, L. N.; Buzdin, A. I.; Kulić, M. L.; Panjukov, S. V., *Adv. Phys.* **1985**, *34*, 175-261.
- (21) X-area, STOE & Cie GmbH: Damstadt, Germany, 2009
- (22) Sheldrick, G., *Acta Crystallogr. A* **2008**, *64*, 112-122.
- (23) Osborn, J. A., *Phys. Rev.* **1945**, *67*, 351-357.
- (24) Tagliati, S.; Rydh, A., *Thermochim. Acta* **2011**, *522*, 66-71.
- (25) Tagliati, S.; Rydh, A.; Xie, R.; Welp, U.; Kwok, W. K., *J. Phys.: Conf. Ser.* **2009**, *150*, 052256.
- (26) Sangster, J.; Pelton, A. D., *J. Phase Equilib.* **1993**, *14*, 243-245.
- (27) Ono, S.; Hui, F. L.; Despault, J. G.; Calvert, L. D.; Taylor, J. B., *J. Less-Common Met.* **1971**, *25*, 287-294.
- (28) Lee, C.-H.; Iyo, A.; Eisaki, H.; Kito, H.; Teresa Fernandez-Diaz, M.; Ito, T.; Kihou, K.; Matsuhata, H.; Braden, M.; Yamada, K., *J. Phys. Soc. Jpn.* **2008**, *77*, 083704.
- (29) Bukowski, Z.; Weyeneth, S.; Puzniak, R.; Karpinski, J.; Batlogg, B., *Phys. C (Amsterdam, Neth.)* **2010**, *470*, S328-S329.
- (30) Golubov, A. A.; Dolgov, O. V.; Boris, A. V.; Charnukha, A.; Sun, D. L.; Lin, C. T.; Shevchun, A. F.; Korobenko, A. V.; Trunin, M. R.; Zverev, V. N., *JETP Lett.* **2011**, *94*, 333.

- (31) Shen, B.; Yang, H.; Wang, Z.-S.; Han, F.; Zeng, B.; Shan, L.; Ren, C.; Wen, H.-H., *Phys. Rev. B* **2011**, 84, 184512.
- (32) Ren, Z.; Zhu, Z.; Jiang, S.; Xu, X.; Tao, Q.; Wang, C.; Feng, C.; Cao, G.; Xu, Z. a., *Phys. Rev. B* **2008**, 78, 052501.
- (33) Jeevan, H. S.; Hossain, Z.; Kasinathan, D.; Rosner, H.; Geibel, C.; Gegenwart, P., *Phys. Rev. B* **2008**, 78, 052502.
- (34) Wenz, P.; Schuster, H. U., *Z. Naturforsch. B* **1984**, 39, 1816-1818.
- (35) Hellmann, A.; Loehken, A.; Wurth, A.; Mewis, A., *Z. Naturforsch. B* **2007**, 62, 155-161.

Table 1. Crystal data and structure refinement for RbEuFe₄As₄ at 293 K.

Empirical formula	RbEuFe ₄ As ₄
Formula weight	760.51 g/mol
Temperature	293 K
Wavelength	0.71073 Å
Crystal system	Tetragonal
Space group	<i>P4/mmm</i>
Unit cell dimensions	$a = 3.8825(3)$ Å, $\alpha = 90^\circ$ $b = 3.8825(3)$ Å, $\beta = 90^\circ$ $c = 13.2733(13)$ Å, $\gamma = 90^\circ$
Volume	200.08(4) Å ³
<i>Z</i>	1
Density (calculated)	6.312 g/cm ³
Absorption coefficient	37.155 mm ⁻¹
<i>F</i> (000)	336
Crystal size	0.210 × 0.163 × 0.090 mm ³
θ range for data collection	3.069 to 29.150°
Index ranges	$-5 \leq h \leq 5$, $-5 \leq k \leq 5$, $-18 \leq l \leq 18$
Reflections collected	1937
Independent reflections	214 [<i>R</i> _{int} = 0.0874]
Completeness to $\theta = 29.150^\circ$	99.5%
Refinement method	Full-matrix least-squares on <i>F</i> ²
Data / restraints / parameters	214 / 0 / 16
Goodness-of-fit	1.372
Final <i>R</i> ^a indices [<i>I</i> > 2σ(<i>I</i>)]	<i>R</i> _{obs} = 0.0336, <i>wR</i> _{obs} = 0.0767
<i>R</i> indices (all data)	<i>R</i> _{all} = 0.0343, <i>wR</i> _{all} = 0.0771
Extinction coefficient	0.012(2)
Largest diff. peak and hole	1.815 and -1.995 e·Å ⁻³

^a $R = \sum ||F_o| - |F_c|| / \sum |F_o|$, $wR = \{ \sum [w(|F_o|^2 - |F_c|^2)^2] / \sum [w(|F_o|^4)] \}^{1/2}$ and $w = 1 / [\sigma^2(F_o^2) + (0.0223P)^2 + 2.0749P]$, where $P = (F_o^2 + 2F_c^2) / 3$

Table 2. Atomic coordinates and equivalent isotropic displacement parameters U_{eq} (\AA^2) for $\text{RbEuFe}_4\text{As}_4$ at 293 K with estimated standard deviations in parentheses.

Label	x	y	z	Occupancy	U_{eq}^*
Eu	0	0	0	1	0.008(1)
As1	0	0	0.3351(2)	1	0.008(1)
As2	0.5	0.5	0.1257(2)	1	0.007(1)
Fe	0	0.5	0.2300(1)	1	0.006(1)
Rb	0.5	0.5	0.5	1	0.013(1)

* U_{eq} is defined as one third of the trace of the orthogonalized U_{ij} tensor.

Figure Captions

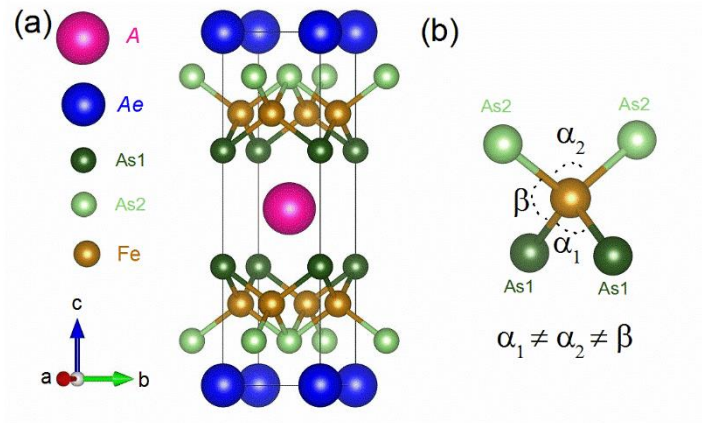


Figure 1. (a) Crystal structure of holed doped superconductors $A Ae Fe_4 As_4$ ($A = K, Rb, Cs$; $Ae = Ca, Sr, Eu$) (b) Local tetrahedral coordination of Fe with three different As-Fe-As bond angles.

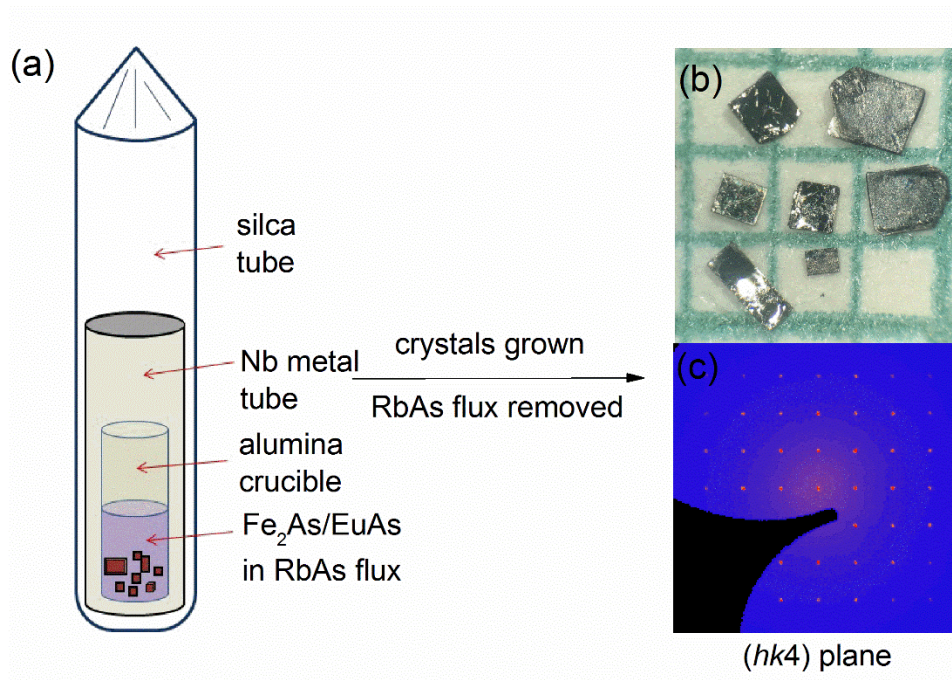


Figure 2. (a) Crucible and tube assemblies for $RbEuFe_4As_4$ crystal growth. (b) Harvested single crystals on a 1-mm grid paper under an optical microscope. (c) Processed image of $(hk4)$ planes in reciprocal space from single crystal x-ray diffraction.

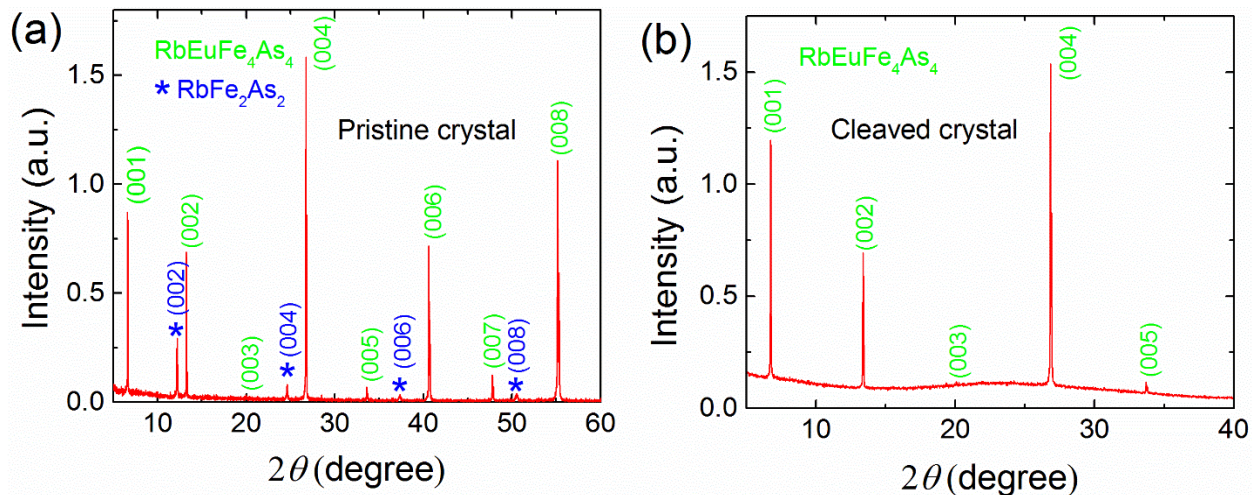


Figure 3. Powder x-ray diffraction profiles of (a) a pristine crystal of $\text{RbEuFe}_4\text{As}_4$ and (b) the same crystal with the surface cleaved off.

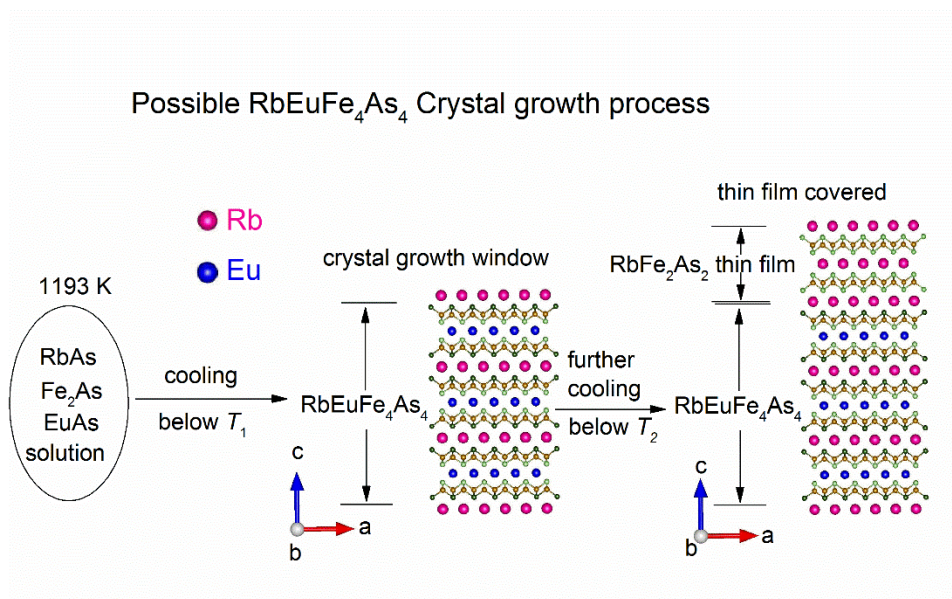


Figure 4. Possible $\text{RbEuFe}_4\text{As}_4$ crystal growth process in a ratio of $\text{RbAs} : \text{Fe}_2\text{As} : \text{EuAs} = 15 : 1 : 1$. T_1 is the temperature when $\text{RbEuFe}_4\text{As}_4$ crystals begin to grow. T_2 is the temperature when thin films of RbFe_2As_2 begin to cover the (001) surface of $\text{RbEuFe}_4\text{As}_4$.



Figure 5. (a) Temperature dependence of ab -planar resistivity of a $\text{RbEuFe}_4\text{As}_4$ single crystal. The lower inset shows a zoom-in of the resistivity near the superconducting transition. (b) Suppression of T_c measured resistively in a single crystal of $\text{RbEuFe}_4\text{As}_4$ with different magnetic fields. (c) Transverse resistivity versus magnetic field at different temperatures.

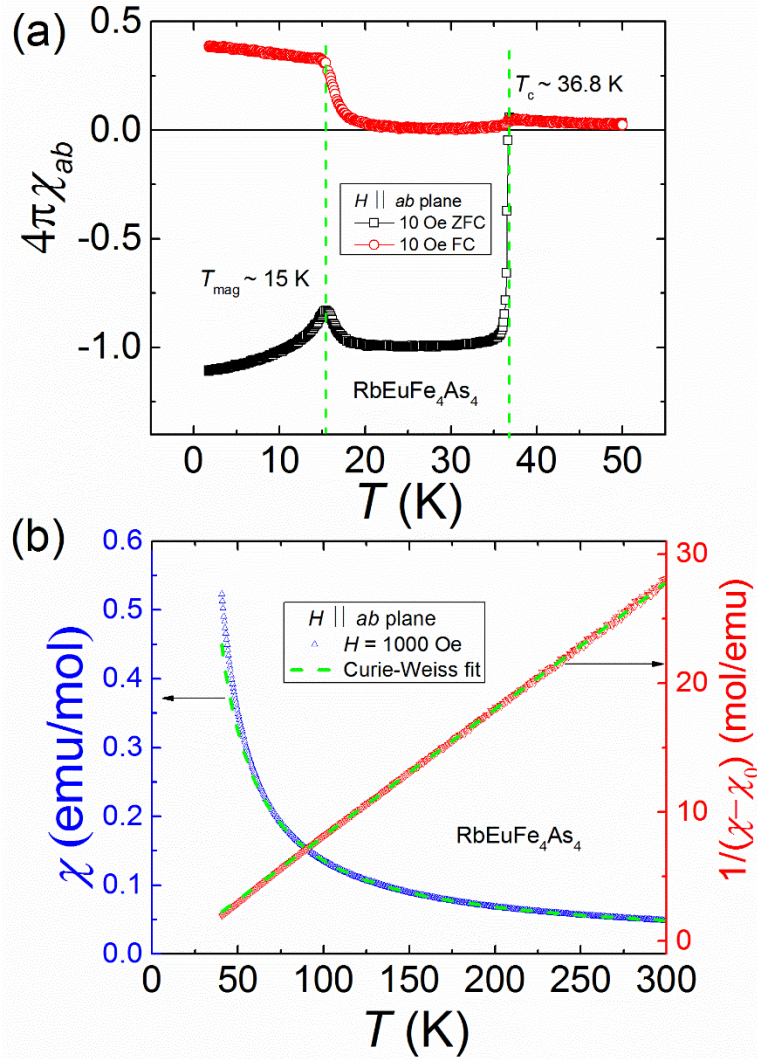


Figure 6. (a) Temperature dependence of magnetic susceptibility of single-crystal $\text{RbEuFe}_4\text{As}_4$ under zero-field-cooled (black) and field-cooled (red) procedures with magnetic fields applied in the ab plane below. The dashed green lines are a guide for the eyes. (b) Temperature dependence of magnetic susceptibility of $\text{RbEuFe}_4\text{As}_4$ above 40 K with a magnetic field $H = 1000$ Oe applied in the ab plane. The dashed green lines are a Curie-Weiss fit.

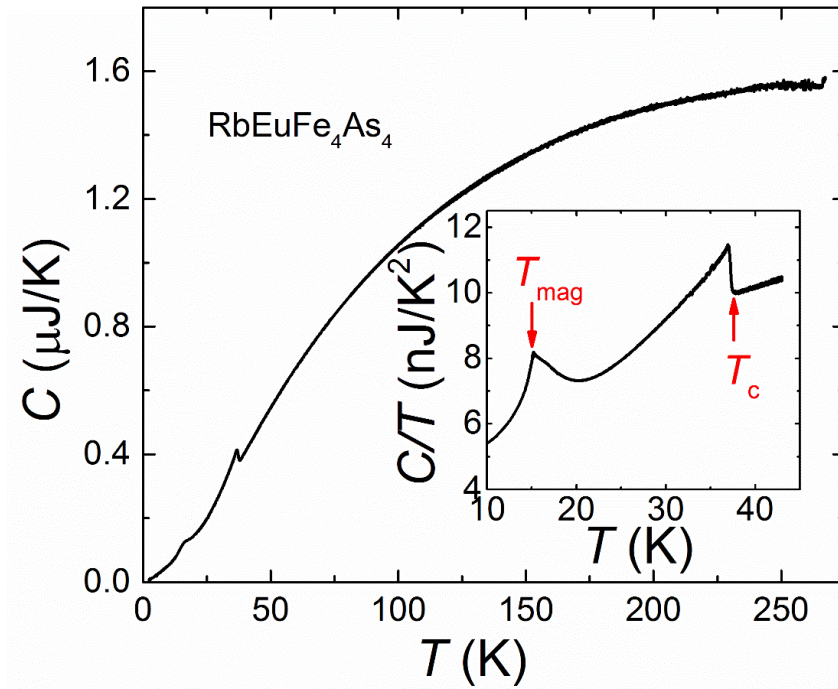
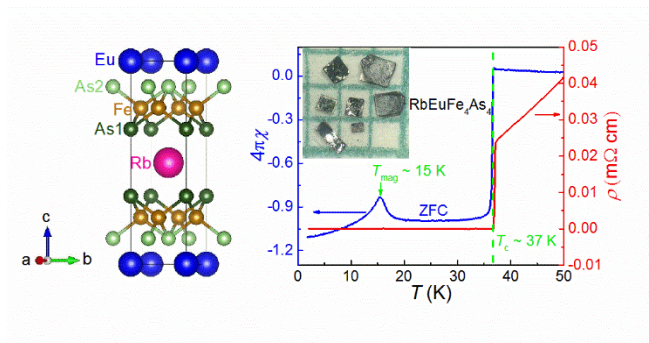


Figure 7. Temperature dependence of specific heat $C(T)$ of $\text{RbEuFe}_4\text{As}_4$. The inset shows C/T vs T in the temperature range where two transitions appear.

For Table of Contents only



Supporting information:

Single crystal growth and study of the ferromagnetic superconductor $\text{RbEuFe}_4\text{As}_4$

Jin-Ke Bao¹, Kristin Willa¹, Matthew P. Smylie¹, Haijie Chen^{1,2}, Ulrich Welp¹, Duck Young Chung¹, and Mercuri G. Kanatzidis^{1,2,*}

¹Materials Science Division, Argonne National Laboratory, Argonne, Illinois 60439, United States, ²Department of Chemistry, Northwestern University, Evanston, Illinois 60208, United States.

*E-mail: m-kanatzidis@northwestern.edu

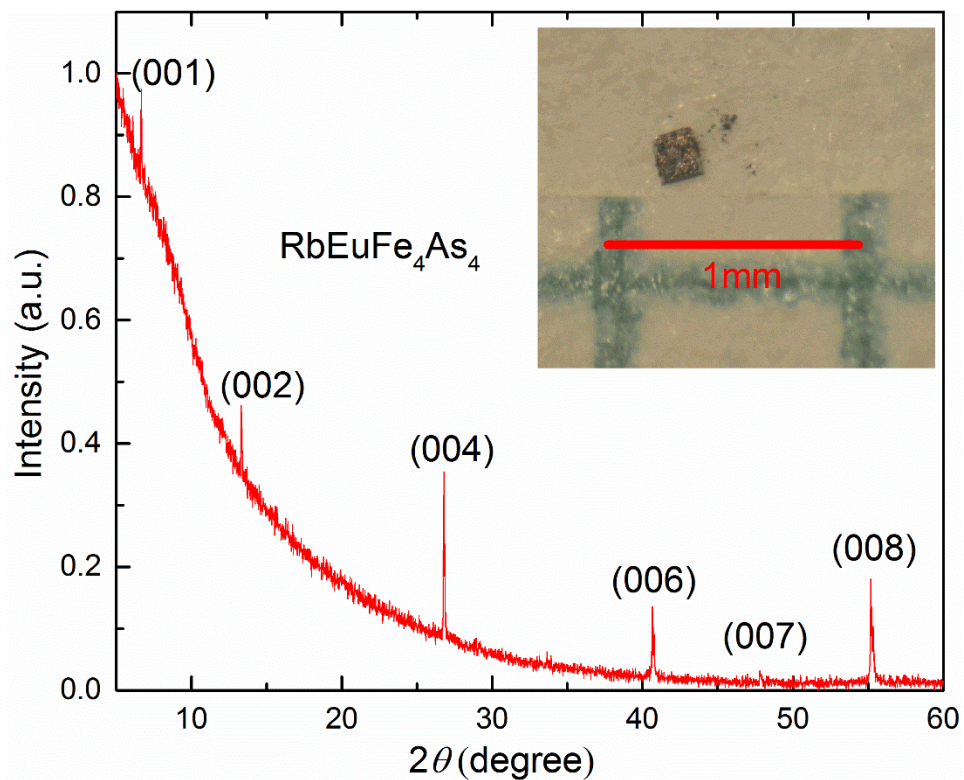


Figure S1 Powder x-ray diffraction of one single crystal RbEuFe₄As₄ grown from the ratio RbAs: EuFe₂As₂ = 5:1. A photo of a tiny crystal with a length of ~ 0.2 mm under an optical microscope.

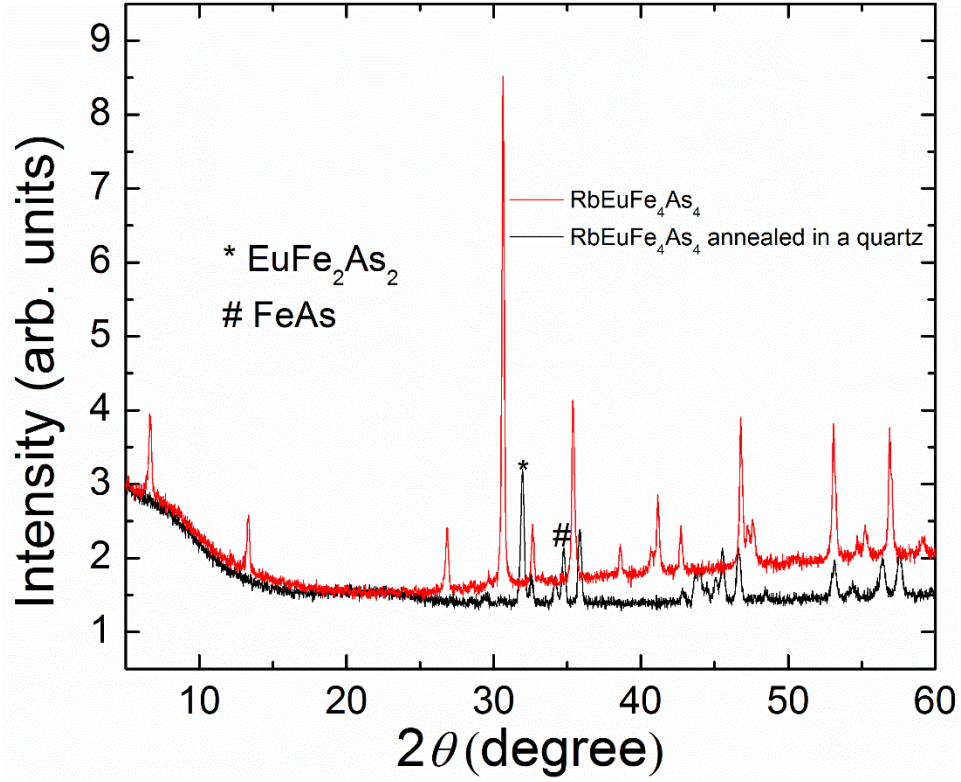


Figure S2 Powder x-ray diffraction of pure $\text{RbEuFe}_4\text{As}_4$ polycrystalline material before and after being annealed at 1173 K in a quartz tube. The main phase after annealing is EuFe_2As_2 and FeAs .

Table S1. Anisotropic displacement parameters U_{ij} ($\text{\AA}^2 \times 10^3$) for $\text{RbEuFe}_4\text{As}_4$ sample A1 at 293 K with estimated standard deviations in parentheses.

Label	U_{11}	U_{22}	U_{33}	U_{12}	U_{13}	U_{23}
Eu	8(1)	8(1)	8(1)	0	0	0
As1	9(1)	9(1)	6(1)	0	0	0
As2	8(1)	8(1)	5(1)	0	0	0
Fe	7(1)	7(1)	6(1)	0	0	0
Rb	15(1)	15(1)	11(1)	0	0	0

The anisotropic displacement factor exponent takes the form: $-2\pi^2[h^2a^{*2}U_{11} + \dots + 2hka^*b^*U_{12}]$.

Table S2. Bond lengths (Å) and bond angles (°) for RbEuFe₄As₄ sample A1 at 293 K with estimated standard deviations in parentheses.

Bond lengths (Å)	
Eu-As2	3.2125(8) × 8
Fe-As1	2.3904(11) × 4
Rb-As1	3.5112(9) × 8
Fe-As2	2.3844(12) × 4
Fe-Fe	2.7453(2) × 4
Bond angles (°)	
As2-Fe-As2	109.01(8)
As2-Fe-As1	109.81(2) × 4
As1-Fe-As1	108.60(7)
As2-Eu-As2	117.43(5) × 4
As2-Eu-As2	62.57(5) × 4
As2-Eu-As2	180.00 × 4
As2-Eu-As2	74.35(2) × 8
As2-Eu-As2	105.65(2) × 8
As1-Rb-As1	180.00 × 4
As1-Rb-As1	112.87(2) × 8
As1-Rb-As1	67.13(2) × 8
As1-Rb-As1	77.13(4) × 4
As1-Rb-As1	102.87(4) × 4

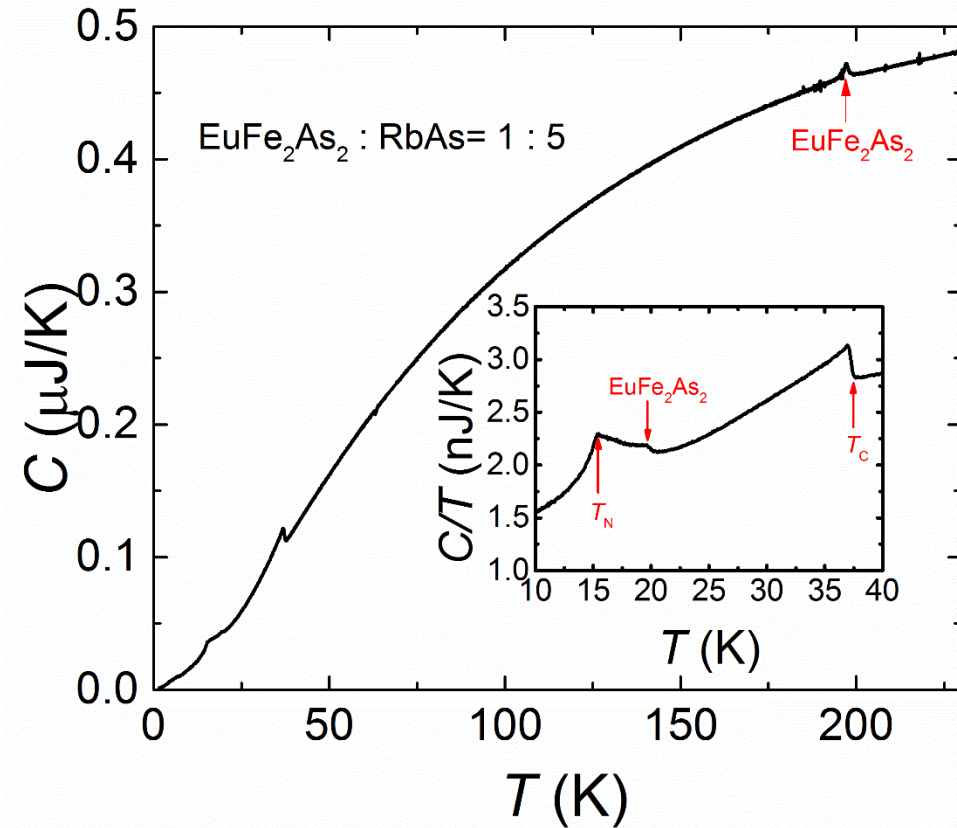


Figure S3 Temperature dependence of specific heat C from the crystals grown in the batch with the ratio $\text{RbAs} : \text{EuFe}_2\text{As}_2 = 5 : 1$. The inset shows C/T vs T from 10 to 40 K. There are two phase transitions at T_N and T_C from the $\text{RbEuFe}_4\text{As}_4$ phase. There are another two transitions at ~ 20 K and 195 K in the same crystal, demonstrating the existence of a tiny impurity phase of EuFe_2As_2 .

Sample label information:

Sample A1 and A2 are crystals from the same batch grown under the condition RbAs : Fe₂As : EuAs = 15 : 1 : 1. The single crystal refinements results in the article are from sample A1. Sample B1 and B2 are crystals from the same batch grown under the condition RbAs : EuFe₂As₂ = 5 : 1.

Table S3 As-Fe-As Bond angles in the FeAs₄ tetrahedron from four different samples.

Sample A1	
Bond angles (°)	
As2-Fe-As2	109.01(8)
As2-Fe-As1	109.81(2) × 4
As1-Fe-As1	108.60(7)
Sample A2	
Bond angles (°)	
As2-Fe-As2	108.93(8)
As2-Fe-As1	109.83(2) × 4
As1-Fe-As1	108.57(8)
Sample B1	
Bond angles (°)	
As2-Fe-As2	108.93(3)
As2-Fe-As1	109.834(11) × 4
As1-Fe-As1	108.56(3)
Sample B2	
Bond angles (°)	
As2-Fe-As2	109.03(5)
As2-Fe-As1	109.764(14) × 4
As1-Fe-As1	108.75(5)

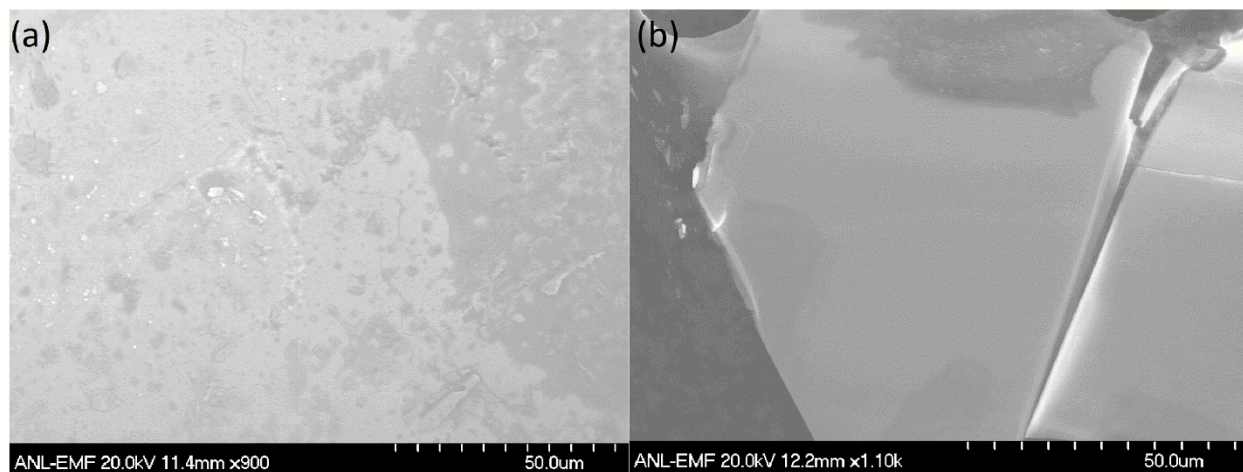


Figure S4 (a), (b) Scanning electron microscope images of one pristine crystal $\text{RbEuFe}_4\text{As}_4$ and another cleaved one, respectively.